Huchon, P., Taylor, B., and Klaus, A. (Eds.)
Proceedings of the Ocean Drilling Program, Scientific Results Volume 180

5. Correlations between Seismic, Logging, and Core Data from ODP Leg 180 Sites in the Western Woodlark Basin[1]

Andrew M. Goodliffe,[2] Brian Taylor,[2] and Garry Karner[3]

ABSTRACT

Synthetic seismograms are constructed from check shot–corrected velocity and density measurements collected during Ocean Drilling Program (ODP) Leg 180 at Sites 1109, 1115, and 1118. The synthetic seismograms facilitate direct correlation of a coincident multichannel seismic (MCS) profile with borehole data collected at the three sites. The MCS data and the synthetic seismograms correlate very well, with most major reflectors successfully reproduced in the synthetics. Our results enable a direct calibration of the MCS data in terms of age, paleoenvironment, and subsidence history. Seismic reflectors are time correlative within stratigraphic resolution but are often observed to result from different lithologies across strike. Our results facilitate the extrapolation of the sedimentation history into an unsampled section of Site 1118 and enable a full correlation between the three sites using all the data collected during ODP Leg 180. This study forms the foundation for regionalizing the site data to the northern margin of the Woodlark Basin, where the transition from continental rifting to seafloor spreading is taking place.

INTRODUCTION

The Woodlark Basin is a young marginal basin in the southwest Pacific that split the orogenically thickened continental crust of southeast

[1]Goodliffe, A.M., Taylor, B., and Karner, G., 2001. Correlations between seismic, logging, and core data from ODP Leg 180 sites in the western Woodlark Basin. *In* Huchon, P., Taylor, B., and Klaus, A. (Eds.), *Proc. ODP, Sci. Results,* 180, 1–25 [Online]. Available from World Wide Web: <http://www-odp.tamu.edu/publications/180_SR/VOLUME/CHAPTERS/167.PDF>. [Cited YYYY-MM-DD]
[2]School of Ocean and Earth Science and Technology, University of Hawaii at Manoa, 2525 Correa Road, Honolulu HI 96822-2285, USA. Correspondence author: **andrew@soest.hawaii.edu**
[3]Lamont-Doherty Earth Observatory, Columbia University, Route 9W, Palisades NY 10964, USA.

Initial receipt: 14 December 2000
Acceptance: 10 May 2001
Web publication: 27 August 2002
Ms 180SR-167

Papua (Taylor et al., 1995) (Fig. F1). Seafloor spreading magnetic anomalies record the creation of oceanic lithosphere since 6 Ma and its propagation westward to Moresby Seamount at present day (Goodliffe, 1998; Taylor et al., 1999). During Ocean Drilling Program (ODP) Leg 180, we drilled 10 sites ahead of the present spreading tip at 151°39′E (Fig. F1) with the goals of characterizing the rift-related subsidence and penetrating the shear zone of a major low-angle fault dipping north from Moresby Seamount (Taylor et al., 1995; Mutter et al., 1996; Abers et al., 1997). Although the latter goal was not fully realized (Shipboard Scientific Party, 1999a), cores recovered from the northern margin (Sites 1118, 1109, and 1115, from south to north) and Moresby Seamount (Sites 1114 and 1116) record the subsidence of the basin since the onset of rifting at ~8 Ma. Cores recovered from the lower section of Site 1115 also record the prerift forearc basin history. This study uses synthetic seismograms to correlate borehole data from Sites 1118, 1109, and 1115 on the northern margin to high-quality multichannel seismic (MCS) data (Goodliffe et al., 1999). This allows the high-resolution subsidence history, from a coastal fluvial environment to the modern-day bathyal depths, to be defined along a crosshole-correlated transect across the margin.

F1. Regional setting of Leg 180 drill sites, p. 12.

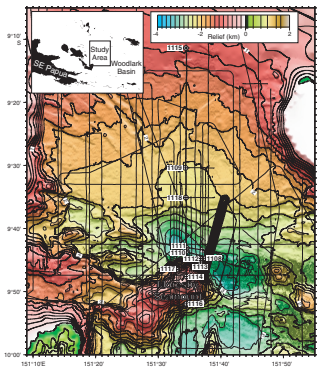

VELOCITY AND DENSITY DATA

Velocity and density profiles were constructed for each of the three sites by merging measurements from downhole logging and lab measurements and editing erroneous values. Preliminary processing of the logging data was carried out during Leg 180 (Taylor, Huchon, Klaus, et al., 1999), with final processing, including depth shifts and corrections for borehole diameter, carried out by the Lamont-Doherty Earth Observatory Borehole Research Group. Downhole logging was carried out at Site 1118 between 891 meters below seafloor (mbsf) and the mudline, at Site 1109 between 786 mbsf and the mudline, and at Site 1115 between 784 mbsf and the mudline. Velocity measurements were made using the array sonic tool in linear mode with the eight-receiver array used in short- and long-spacing modes to provide full waveform analysis. The logging velocity (DTCO), derived from coherence of the full eight waveforms, was used in preference to the short- and long-spacing data because of the lower levels of noise and closer agreement with shipboard velocity measurements. Downhole density (RHOM) measurements were made using the hostile environment lithodensity sonde, using a gamma ray source to determine the electron density of the formation. Quality control of the logging velocity and density data made extensive use of the caliper log (LCAL) (Shipboard Scientific Party, 1999b, 1999c, 1999d) to determine the location of washouts, where the caliper became fully extended and potentially out of contact with the borehole wall. Data from such locations were considered unreliable and were therefore discarded. Unreasonable values of density and velocity (such as those that recorded the properties of the drilling fluid) were also discarded.

Two sources of laboratory *P*-wave velocity measurements were used. The PWS1 and PWS2 insertion probe system was used for unconsolidated sediments (Blum, 1997). This provided measurements of the longitudinal (along the core axis) and transverse (across the core axis) velocity, respectively, based on a fixed distance and measured acoustic signal transit time. In semilithified sediments and rock cores, the PWS3

contact probe system (Boyce, 1976; Blum, 1997) was employed. The PWS3 system accommodates a variable sample thickness, which is measured in addition to transit time and can be used to measure velocity on split cores (across the core axis) or individual samples (in any orientation). When PWS1, PWS2, and PWS3 velocities were available for a single sample, we found that the PWS1 and PWS2 velocities were an average of 40 m/s slower than the PWS3 measurements. As the cores were not oriented, PWS1 and PWS3 velocity measurements should on the average be equal, thus indicating an instrumental error of ~40 m/s. As the PWS3 measurements were found to be in close agreement with the DTCO velocities, 40 m/s was added to the PWS1 and PWS2 velocities to make them approximate the PWS3 velocity (and therefore the logging velocity). For the data compilation, the more reliable PWS3 measurements were used when possible. PWS1 measurements (the longitudinal velocity better simulating logging measurements) were used in places not measured by the PWS3 probe. PWS1, PWS2, and PWS3 velocities were taken, on average, every 1.7 m, sediment type allowing. Laboratory measurements of bulk density were obtained during routine measurement of index properties. The sample interval averaged 2.25 m.

The combination of shipboard and logging data that went into making composite velocity and density profiles for each site is shown in Tables T1 and T2. For all sites, outlier values (e.g., unexplainable spikes or densities/velocities below that of water) were removed from the composite profiles before the data were resampled to 0.5 m by linear interpolation. No special treatment had to be given to the merge points between the shipboard and downhole measurements, as the data scatter in the shipboard measurements exceeded any consistent differences between the two data sets. No artifacts were seen in the synthetic seismograms resulting from these merge points. Special consideration was given to Site 1118, where the first 205 m of Hole 1118A was drilled without coring. At this site, logging data did not extend above 100 mbsf. Above 100 mbsf, shipboard measurements of density from Site 1109 were used. A 25-m Gaussian filter was applied to remove artifacts in the synthetic seismogram resulting from merging the two data sets from different sites.

T1. Depth intervals used to create composite velocity profiles, p. 20.

T2. Depth intervals used to create composite density profiles, p. 21.

VERTICAL SEISMIC PROFILES AND CHECK-SHOT CORRECTIONS

The DLIS-format vertical seismic profile (VSP) data were imported into Landmark's MCS ProMAX processing package to perform quality control and first-break picks on the surface hydrophone and downhole receiver data. Quality control included the inspection of pre- and post-stack data for excessive noise from external sources or downhole tool motion after the calipers had been clamped at a station in the hole. Transit times were corrected for the depth of the air gun, separation of the air gun and the surface hydrophone, elevation of rig floor above sea level, and horizontal separation of the downhole hydrophone and the air gun. The resultant one-way traveltimes are zero offset with respect to sea level. Check-shot corrections were applied to the velocity profiles derived above by dividing the one-way traveltime between two check-shot depths (T') by the one-way traveltime derived from the composite velocity profile for the same depth interval (T). Multiplying the result (C) by each velocity value in our composite profile for that interval

yielded velocities (V) that gave a depth-to-time conversion consistent with the check-shot information:

$$T = \sum_{i=\text{depth1}}^{\text{depth2}} \text{velocity}(i) \times \text{factor},$$

$$T' = (\text{time 2} - \text{time 1})/2,$$

$$C = T'/T, \text{ and}$$

$$V = C \times \text{velocity},$$

where

T = total one-way traveltime between depth 1 and depth 2 from the check-shot data,
factor = conversion of velocity values to time, and
T' = total one-way traveltime between depth 1 and depth 2 from the composite velocity profile.

Specific information for each site is given below. No attempt was made to correct velocities below the deepest check shot at any of the three sites.

Site 1118

Twenty levels between 142.3 and 682.3 mbsf were occupied during the VSP survey at Site 1118. A combination of optimizing signal-to-noise ratio and distributing check shots throughout the borehole resulted in the selection of check shots at 265.3, 415.3, and 685.3 mbsf, corresponding to two-way traveltimes of 318.32, 474.36, and 739.36 ms, respectively. Check-shot corrections increased velocity by 3.14% between 0 and 265.3 mbsf, decreased it by 2.41% between 265.3 and 415.3 mbsf, and decreased it by 0.85% between 415.3 and 685.3 mbsf.

Site 1109

The VSP recorded at Site 1109 occupied nine levels in the borehole between 378.9 and 460.3 mbsf. Of these, only the records from 398.9 and 408.9 mbsf had a high enough signal-to-noise ratio to allow a reliable first-break pick. As a very minor error in first-break time can lead to a large error in interval velocity over a short depth interval, only the check shot recorded at 398.9 mbsf was used. The two-way traveltime for this depth interval was 474.33 ms. The resultant check-shot correction increased the velocities over the interval of 0 to 398.9 mbsf by 2.08%.

Site 1115

The VSP recorded at Site 1115 occupied 16 levels in the borehole between 315.2 and 552.2 mbsf. Problems with the heave compensator and an unidentified source of noise resulted in only two closely spaced depth intervals with a high enough signal-to-noise ratio. The check shot at 552.2 mbsf yielded a two-way traveltime of 645.16 ms and resulted in velocities between 0 and 552.2 mbsf increasing by 0.4%.

SYNTHETIC SEISMOGRAMS

The reflection coefficient, needed to generate the synthetic seismograms, was calculated from the check shot–corrected velocity data and the density data for each site. The resultant files were converted to log ASCII standard (LAS) format and input into ProMAX, where the data were converted from depth to time.

MCS data for each of the three sites were collected on the *Maurice Ewing* in 1995 using a 20 air-gun tuned source array and a 5-km streamer (Goodliffe et al., 1999). The seismic source signal was derived separately for each of the three sites from the stacked and migrated data proximal to each site. Using ProMAX, the seafloor at each site was flattened along the negative-to-positive transition directly before the first positive peak associated with the seafloor. The traces were stacked, and the portion of the signal from the first break to a point interpreted as the end of the source signal, typically ~100 ms, was extracted. The source signal was convolved with the reflection coefficient, and the resultant synthetic seismograms were output with automatic gain control (AGC) applied (200 ms). No attempt was made to include the effects of peg-leg multiples.

RESULTS

Figure F2 shows the synthetic seismograms and MCS data along line EW95-1366 for Sites 1118, 1109, and 1115. A 200-ms AGC window has been applied to both data sets. The units defined herein for Sites 1118, 1109, and 1115 (Figs. F3, F4, F5; organized south–north on the northern margin) are consistent with regional seismic stratigraphic units that exist beyond line EW95-1366 (Fig. F2) (Taylor et al., unpubl. data). Tables T3, T4, and T5 present the depth, age, and two-way traveltime of the boundaries between these units, key reflectors described herein, and bio- and magnetostratigraphic markers (Takahashi et al., this volume). The corresponding density, check shot–corrected velocity, and reflection coefficient profiles are presented in Figs. F3, F4, and F5. To aid in cross-site correlations, the lithostratigraphic units, paleodepth, and age-depth curves (with symbols projected into two-way traveltime) are also shown (Shipboard Scientific Party, 1999b, 1999c, 1999d; Takahashi et al., this volume).

Most of the major features of the MCS data in the vicinity of each site are well reproduced by the synthetic seismograms, confirming the accuracy of the density and check shot–corrected velocity profiles. Check-shot results show that the maximum error in the initial velocity profiles was ~3.14% (2.41% if the top of Site 1118, where data was extrapolated from Site 1109, is ignored), with a mean of 0.55% (not including any estimate of error beneath the deepest check shots). Some of this error may be due to shipboard measurements of velocity underestimating in situ velocities resulting from loss of overburden (Hamilton, 1979; Fulthorpe et al., 1989; Urmos et al, 1993). The results also show that the source signal has been well characterized, a key step in obtaining good synthetic seismograms. The source signal dominates for approximately the first 70 ms of the synthetic seismogram (the approximate length of the source signal at peak amplitude). In this interval, it is difficult to extract any geological information from the MCS data. This represents, on average, the top 55 m of each site, or a little over 1 m.y. of depositional history.

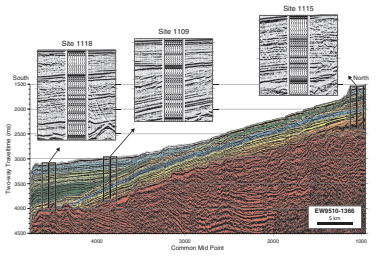

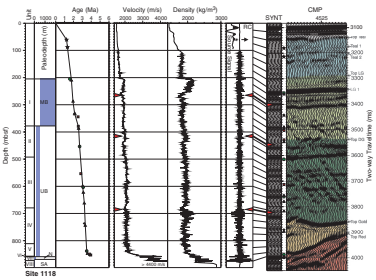

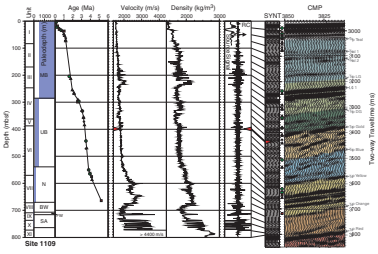

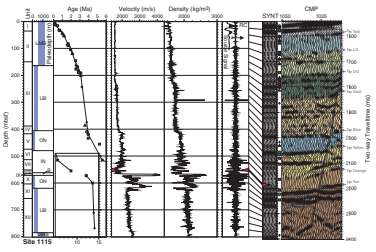

The discussion below details the correlation of prominent reflectors between Sites 1118, 1109, and 1115 (Figs. F3, F4, F5). It should be noted when interpreting these results that the synthetic seismograms presented herein are minimum phase (i.e., the first break of the waveform is coincident with the causative spike in the reflection coefficient). For example, the main positive peak of the seafloor reflection in the synthetic seismogram for Site 1118 is centered on ~3100 ms. However, the seafloor is actually at 3083 ms. At 1500 m/s, this is a difference of 12.75 m. Seismic correlations typically pick the main positive peak of a reflector, but this time would only represent the causative event if the waveform were zero phase. This is commonly not the case with seismic reflection data, which are typically minimum phase; therefore, the physical feature causing the event is at the first break. To aid in assigning ages to particular seismic reflectors, the biostratigraphic, magnetostratigraphic, and radioisotope ages of samples in depth have been presented in two-way traveltime between the synthetic and MCS data in Figures F3, F4, and F5. A shift of 18 ms at Sites 1118 and 1115 and 22 ms at Site 1109 (the lag between the first break and the peak amplitude of the first positive spike in the source signal) has been added to the two-way traveltime of the stratigraphic markers, facilitating direct correlation.

DISCUSSION

The first-order seismic correlations between drilled Sites 1118, 1109, and 1115 can be seen on Figure F2. Dolerite basement was intersected at Sites 1109 and 1118 (Red unit), whereas samples recovered from below ~2200 ms at Site 1115 record a history of forearc basin sedimentation (Tan unit). An unconformity above these units is onlapped successively by the Orange, Yellow, and Blue units, intersected at Sites 1109 and 1115. Increasing subsidence tilted these units to the south, producing a margin slope that received hemipelagic sediments at the same time as turbidites lapped northward and resulted in the differential sedimentation recorded by the Gold through Teal units. Submarine channels (Fig. F1) formed during this time and selectively eroded parts of these units, as seen in Figure F2 between Sites 1109 and 1115.

No samples were recovered at Site 1118 between 0 and 205.0 mbsf, as this section was drilled without coring. Age estimates can be extrapolated into this interval by correlation with Site 1109. A pair of reflectors (Teal 1 and Teal 2) in the middle of the Teal unit can be directly correlated (Fig. F2) between Site 1118 (Fig. F3) and Site 1109 (Fig. F4). At Site 1109, the reflectors are at 3086 and 3114 ms; their causative events are 22 ms higher. The time-to-depth function derived for this site indicates that the corresponding depths are 79.63 and 102.08 mbsf. Interpolation of the results of Takahashi et al. (this volume) assigns ages of 1.23 and 1.32 Ma. At Site 1118, these reflectors are at 3180 and 3214 ms, corresponding to an event at 3162 and 3196 ms. The depth-to-time function for this site assigns depths of 60.83 and 87.53 mbsf, which, assuming that the reflectors are time correlative as elsewhere, can be assigned the ages of 1.23 and 1.32 Ma (Tables T3, T4).

At Site 1118, the first prominent reflector in the Light Green (LG) unit (Fig. F3; LG 1) is directly correlatable to Site 1109 (Fig. F4; LG 1). This reflector is well reproduced in the synthetic data for each site. The synthetic seismogram for Site 1118 shows that this reflector is the result of the top of a prominent horizon at 204 mbsf distinguished by an

abrupt increase in velocity and density. Logging and sparse samples define this interval as continuing to 255.5 mbsf and having a lithology that is predominantly silty at the bottom, grading upward into a formation of primarily clay (Shipboard Scientific Party, 1999d). The MCS data over this depth interval show that the bottom of this unit, as well as some internal structure, may also be resolved. The vertical seismic resolution ($\lambda/4$) indicated by the source wavelet is ~19 m, indicating that the entire unit should be resolvable. At Site 1109, the LG-1 reflection results from the top of a unit at 219 mbsf with unusually high velocity and density. A contribution to the reflector may also arise from a velocity and density peak at 210 mbsf. From logging data, this unit is interpreted to comprise a thin carbonate layer grading upward into thick sand characterized by high gamma ray counts. Samples of unusually dark sand with some fragments of wood were recovered from this interval, with the presence of volcanic material implied from a very high thorium/uranium ratio (Shipboard Scientific Party, 1999b). The bottom of the unit is at 234 mbsf. The MCS and synthetic data only detect the top of this unit, with no internal structure recorded. Simple interpolation of the results of **Takahashi et al.** (this volume) date this reflector as 1.74 Ma at Site 1118 and 1.76 Ma at Site 1109 (Tables **T3, T4**). This horizon is closely time correlative and formed in a middle bathyal setting at both sites. The associated MCS reflector is continuous between the two sites, despite the varying lithology.

Reflectors above the seismic Blue unit cannot be correlated directly between Sites 1109 and 1115 (Fig. **F2**). Some, such as LG 1, onlap the slope to the north. Others are partially or wholly removed by channel erosion. For these units, therefore, we use the detailed chronostratigraphy to identify time-correlative reflectors at Site 1115 (Fig. **F5**). For example, the 1.76-Ma reflector at Site 1109 (Fig. **F4**) can be correlated with the top of the Olduvai Chron (1.77 Ma), seen at 90.5 mbsf at Site 1115 (Fig. **F5**) (Shipboard Scientific Party, 1999c).

Reflectors above the Blue unit record sedimentation during subsidence of the basin from upper to middle bathyal depths. The Gold, Dark Green (DG), Light Green, and Teal units successively onlap to the north in a shingled pattern (Figs. **F2, F3, F4**). The DG and LG units are thicker by a factor of three at Site 1118 relative to Site 1109. The onlap does not represent an unconformity in time but rather a lateral and vertical change in depositional style from basin turbidites to hemipelagic drape (Shipboard Scientific Party, 1999a).

The top of the Gold unit is a continuous reflector that can be traced between Sites 1118 and 1109. At Site 1118, the reflector occurs at 700 mbsf, below an increase in density and velocity values from 680 mbsf. At Site 1109, the synthetic seismogram shows that the reflector originates from a segment of the reflection coefficient preceding a similar density and velocity increase and is probably caused by a local velocity low at ~350 mbsf. Interpolation of the results of **Takahashi et al.** (this volume) date the top of the Gold unit as 3.28 and 3.22 Ma at Sites 1118 and 1109, respectively (Tables **T3, T4**). This reflector can be correlated to Site 1115 using a sample containing a $^{40}Ar/^{39}Ar$ age of 3.23 ± 0.08 Ma that was found at 243.43 mbsf (Lackschewitz et al., in press) just below a reflector at 1850 ms at Site 1115 (Fig. **F5;** Top Gold). Interpolation of sedimentation rates independent of this age (**Takahashi et al.,** this volume) dates this reflector as 3.23 Ma. It is associated with a downhole variation of velocities and densities very similar to that observed at Site 1118.

The top of the Blue unit (Top Blue; Figs. F4, F5) is dated by foraminifers as 3.5 Ma at Site 1109 and by interpolation between $^{40}Ar/^{39}Ar$ measurements as 3.41 Ma at Site 1115 (Takahashi et al., this volume). At Site 1109, the Blue unit is equivalent to the lower part of lithologic Unit VI. The photoelectric log data for the lower part of this unit (Shipboard Scientific Party, 1999b) show that it can be distinguished on the basis of increasing carbonate content, resulting in a gradual increase in velocity. At Site 1115, the bottom of the Blue unit coincides with lithologic Unit IV, a calcareous sandy silty claystone. A rapid increase in carbonate content at the bottom of Unit IV, as shown by the photoelectric effect log (Shipboard Scientific Party, 1999c), coincides with an increase in density and velocity.

The top of the Yellow unit at Site 1115 coincides with an increase in density and velocity at the base of lithologic Unit IV. Peaks in velocity and density within the Yellow unit are shown by the photoelectric effect log to be caused by local increases in the carbonate content (Shipboard Scientific Party, 1999c). At Site 1109, a gradual increase in density and velocity, with a localized density low at ~540 mbsf, marks the top of the Yellow unit. At both sites, the top of the Yellow unit correlates with a change from upper-bathyal to neritic environments. At Site 1115, the base of the unit may shoal to a marine lagoonal or nearshore wave-worked environment (Shipboard Scientific Party, 1999c). The age of the top of the unit (Figs. F4, F5; Top Yellow) is estimated at 3.8 Ma (3.74 Ma at Site 1109 and 3.87 Ma at Site 1115) (Takahashi et al., this volume).

The top of the Orange unit at Site 1109 is coincident with a sharp decrease in velocity and density, largely due to a decrease in carbonate content associated with brackish and freshwater deposits. Local spikes in velocity may be due to goethite and carbonate concretions (Shipboard Scientific Party, 1999b). At Site 1115, the top of the Orange unit is poorly defined in the MCS data. A velocity drop similar to that at Site 1109 is present, although less sharply developed. At Site 1109, this unit represents a downward transition from a brackish water lagoonal to a subareal environment, with an intervening period of freshwater deposition. At Site 1115, a marine lagoonal environment grades downward into a possible fluvial or beach environment (Shipboard Scientific Party, 1999b, 1999c). At Site 1109, no dates were obtained within the Orange unit or below. The top of the Orange unit is dateable only as older than 5.23 Ma. The results of Takahashi et al. (this volume) imply an age of 5.39 Ma for the top of the Orange unit at Site 1115 (Table T5; Top Orange).

At Site 1115, a conglomerate with sandstone and siltstone is the cause of a large peak in density and velocity between 565.7 and 571.9 mbsf. The associated spike in the reflection coefficient creates a reflection in the synthetic seismogram at ~2220 ms that is coincident with the top of the Tan unit. The thin unit causing this reflection probably marks local sedimentation prior to the onset of rifting in this region (Taylor, Huchon, Klaus, et al., 1999). A nannofossil identified from sediments just above this unit was dated as ≤8.6 Ma (Shipboard Scientific Party, 1999c). The Tan unit records the last stages of the depositional history of a forearc basin (Taylor, Huchon, Klaus, et al., 1999) that does not have an analog at Sites 1118 and 1109.

At Sites 1109 and 1118, the sharp peaks in reflection coefficient starting at ~740 and 860 mbsf, respectively, derive from the igneous conglomerates and the underlying dolerite basement. The resultant reflectors in the synthetic seismograms and MCS data mark the top of

the Red unit. This unit represents the Paleocene ophiolitic basement that has analogs on the Papuan mainland (Baldwin et al., 2000) and in commercial wells to the west (Tjhin, 1976; Francis et al., 1987) and is implied to underlay the forearc basin sediments encountered at the bottom of Site 1115.

CONCLUSIONS

1. Correlations between seismic, logging, and core data from ODP Leg 180 at Sites 1109, 1115, and 1118 have been established by creating synthetic seismograms from a combination of downhole and shipboard measurements of density and check shot–corrected velocity data.
2. The synthetic seismograms successfully reproduce most of the major reflectors in the MCS data, confirming the accuracy of the composite velocity and density data for each site.
3. The detailed biostratigraphy and magnetostratigraphy available for each site permit detailed age and paleoenvironmental parameters to be placed on interpreted seismic horizons that are consistent between the three sites.
4. At Sites 1118 and 1109, where correlations can be made with the least ambiguity, seismic reflectors are time correlative within stratigraphic resolution (~0.1 m.y.) and maintain a similar character between sites. However, the lithology commonly varies.
5. Using the results presented herein, the dated horizons intersected at Sites 1109, 1115, and 1118 can now be extended regionally using an extensive database of regional seismic reflection data.

ACKNOWLEDGMENTS

We would like to thank the crew and scientific staff of the *JOIDES Resolution*. Support was provided by USSAC for postcruise data analysis and interpretation. Illustrations were created using Generic Mapping Tools (Wessel and Smith, 1998).

REFERENCES

Abers, G.A., Mutter, C.Z., and Fang, J., 1997. Shallow dips of normal faults during rapid extension: earthquakes in the Woodlark-D'Entrecasteaux rift system, Papua New Guinea. *J. Geophys. Res.,* 102:15301–15317.

Baldwin, S.L., Montelone, B., Hill, E.J., Ireland, T., and Fitzgerald, P.G., 2000. Continental extension in the western Woodlark Basin, Papua New Guinea, *Trans. Am. Geophys. Union,* 81(48):1307.

Blum, P., 1997. Physical properties handbook: a guide to the shipboard measurement of physical properties of deep-sea cores. *ODP Tech. Note,* 26 [Online]. Available from World Wide Web: <http://www-odp.tamu.edu/publications/tnotes/tn26/INDEX.HTM>. [Cited 2000-12-05]

Boyce, R.E., 1976. Definitions and laboratory techniques of compressional sound velocity parameters and wet-water content, wet-bulk density, and porosity parameters by gravimetric and gamma-ray attenuation techniques. *In* Schlanger, S.O., Jackson, E.D., et al., *Init. Repts. DSDP,* 33: Washington (U.S. Govt. Printing Office), 931–958.

Francis, G., Lock, J., and Okuda, Y., 1987. Seismic stratigraphy and structure of the area to the southeast of the Trobriand Platform. *Geo-Mar. Lett.,* 7:121–128.

Fulthorpe, C.S., Schlanger, S.O., and Jarrard, R.D., 1989. In situ acoustic properties of pelagic carbonate sediments on the Ontong Java Plateau. *J. Geophys. Res.,* 94:4025–4032.

Goodliffe, A.M., 1998. The rifting of continental and oceanic lithosphere: observations from the Woodlark Basin [Ph.D. thesis]. Univ. Hawaii, Honolulu.

Goodliffe, A.M., Taylor, B., and Martinez, F., 1999. Data report: marine geophysical surveys of the Woodlark Basin region. *In* Taylor, B., Huchon, P., Klaus, A. et al., *Proc. ODP Init. Repts.,* 180, 1–20 [CD-ROM]. Available from: Ocean Drilling Program, Texas A&M University, College Station, TX 77845-9547, U.S.A.

Hamilton, E.L., 1979. Sound velocity gradients in marine sediments. *J. Acoust. Soc. Am.,* 65:909–922.

Lackschewitz, K.S., Bogard, P.V.D., and Mertz, D.F., in press. $^{40}Ar/^{39}Ar$ ages of fallout tephra layers and volcaniclastic deposits in the sedimentary succession of the western Woodlark Basin, Papua New Guinea: the marine record of Miocene-Pleistocene volcanism. *In* Wilson, R.C.L., Whitmarsh, R., Taylor, B., and Froitheim, N., *Geol. Soc. Lond. Spec. Pub., Non-volcanic rifting of continental margins: a comparison of evidence from land and sea.* [**N1**]

Mutter, J.C., Mutter, C.Z., and Fang, J., 1996. Analogies to oceanic behavior in the continental breakup of the western Woodlark Basin. *Nature,* 380:333–336.

Shipboard Scientific Party, 1999a. Leg 180 summary. *In* Taylor, B., Huchon, P., Klaus, A., et al., *Proc. ODP, Init. Repts.,* 180: College Station, TX (Ocean Drilling Program), 1–77.

————, 1999b. Site 1109. *In* Taylor, B., Huchon, P., Klaus, A., et al., *Proc. ODP Init. Repts.,* 180, 1–298 [CD-ROM]. Available from: Ocean Drilling Program, Texas A&M University, College Station, TX 77845-9547, U.S.A.

————, 1999c. Site 1115. *In* Taylor, B., Huchon, P., Klaus, A., et al., *Proc. ODP Init. Repts.,* 180, 1–226 [CD-ROM]. Available from: Ocean Drilling Program, Texas A&M University, College Station, TX 77845-9547, U.S.A.

————, 1999d. Site 1118. *In* Taylor, B., Huchon, P., Klaus, A., et al., *Proc. ODP Init. Repts.,* 180, 1–213 [CD-ROM]. Available from: Ocean Drilling Program, Texas A&M University, College Station, TX 77845-9547, U.S.A.

Taylor, B., Goodliffe, A., Martinez, F., and Hey, R., 1995. A new view of continental rifting and initial seafloor spreading. *Nature,* 374:534–537.

Taylor, B., Goodliffe, A.M., and Martinez, F., 1999. How continents break up: insights from Papua New Guinea. *J. Geophys. Res.,* 104:7497–7512.

Taylor, B., Huchon, P., Klaus, A., et al., 1999. *Proc. ODP, Init. Repts.,* 180 [CD-ROM]. Available from: Ocean Drilling Program, Texas A&M University, College Station, TX 77845-9547, U.S.A.

Tjhin, K.T., 1976. Trobriand Basin exploration, Papua New Guinea. *APEA J.,* 81–90.

Urmos, J., Wilkens, R.H., Bassinot, F., Lyle, M., Marsters, J.C., Mayer, L.A., and Mosher, D.C., 1993. Laboratory and well-log velocity and density measurements from the Ontong Java Plateau: new in-situ corrections to laboratory data for pelagic carbonates. *In* Berger, W.H., Kroenke, L.W., Mayer, L.A., et al., *Proc. ODP, Sci. Results,* 130: College Station, TX (Ocean Drilling Program), 607–622.

Wessel, P., and Smith, W.H.F., 1998. New, improved version of the Generic Mapping Tools released. *Eos,* 79:579.

Figure F1. Regional setting of the Leg 180 drill sites. Sites 1118, 1109, and 1115 are on MCS line EW9510-1366, a segment of which (bold black line) is presented in Figure F2, p. 13. Thin black lines indicate the location of regional seismic reflection data. HAWAII-MR1 side-scan data is overlain on bathymetry illuminated from the north (Goodliffe et al., 1999). The two westernmost spreading segments are evident from the high backscatter region trending east–west near 9°50′S on the eastern side of the plot. The bathymetry contour interval is 200 m, labeled in kilometers.

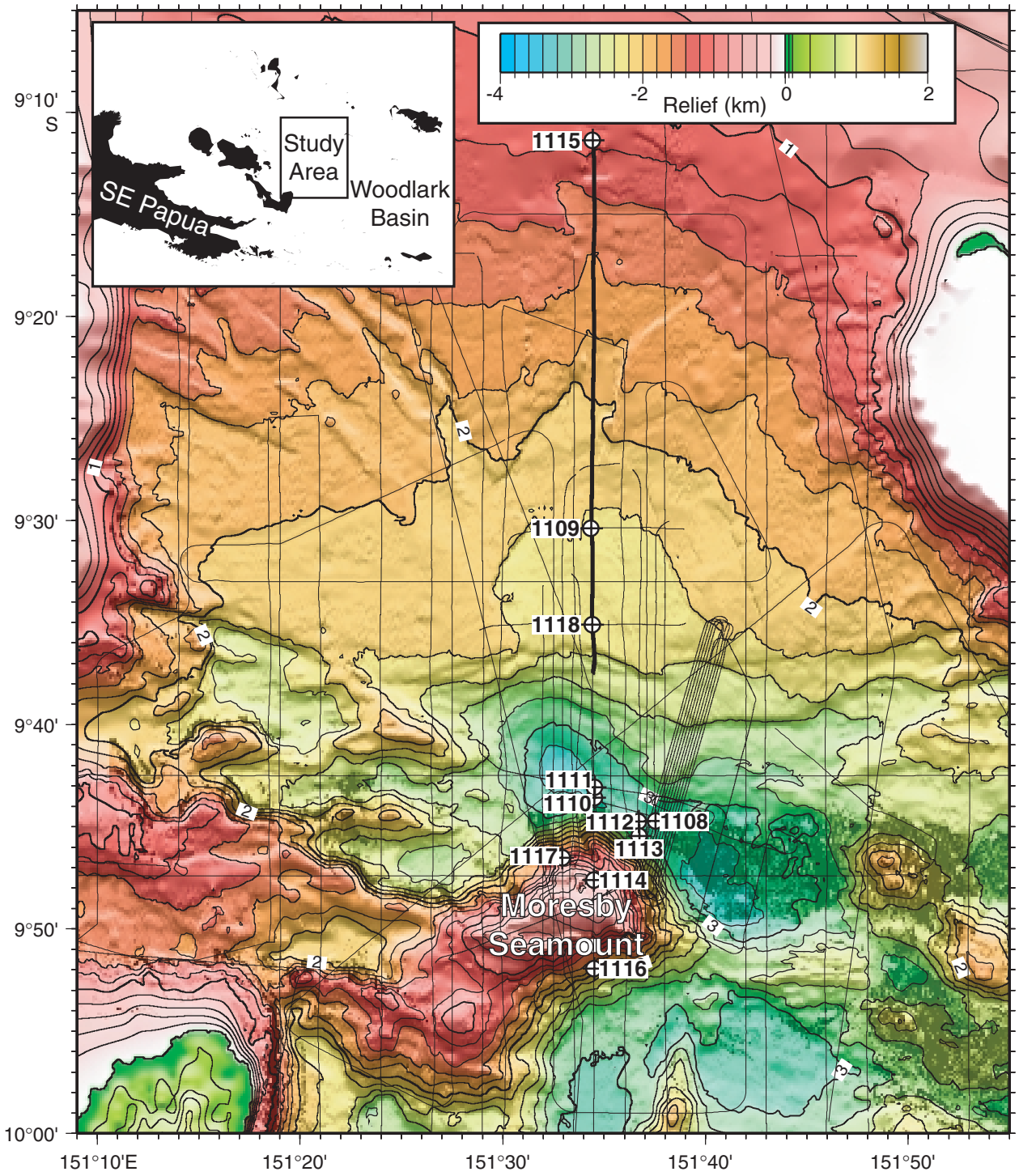

Figure F2. MCS line EW9510-1366 is presented for the region of Sites 1118, 1109, and 1115. Boxes on the seismic data indicate the location of the corresponding insets within which the MCS data have been split at the common midpoint corresponding to the site and synthetic seismograms inserted. The bold line in the center of each location box indicates the interval drilled.

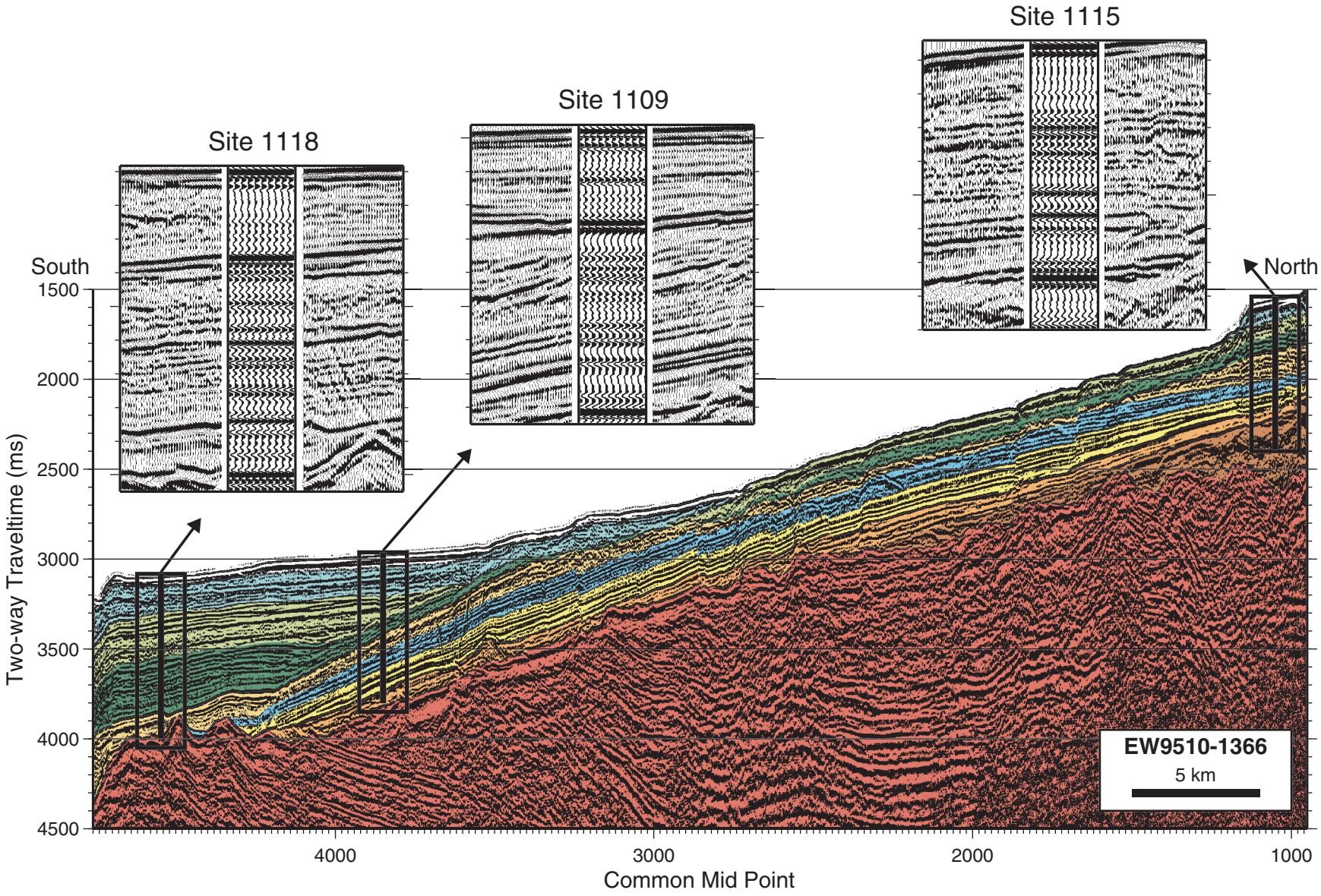

Figure F3. Logging and coring results (Shipboard Scientific Party, 1999d), check shot–corrected depth conversion, and correlation via synthetic seismogram to MCS data in the vicinity of Site 1118. From left to right, the first panel (Unit) gives the lithologic units defined at Site 1118. The second panel shows the paleoenvironment interpreted from the biostratigraphic results. MB = middle bathyal, UB = upper bathyal, N = neritic, SA = subaerial. Panel three details the age and subsidence history recorded at Site 1118. Stars = correlations with Site 1109 derived from seismic reflection line EW9510-1366 (Fig. **F2,** p. 13) in the absence of sampling in the upper part of the hole. Circles = foraminiferal ages, triangles = magnetostratigraphic ages, squares = nannofossil ages, crosses = $^{40}Ar/^{39}Ar$ ages (Lackschewitz et al., in press). The depth-age relationship (**Takahashi et al.,** this volume) is shown by the black line. Panels four and five detail the integrated velocity and density profiles derived from downhole and shipboard measurements. The three arrows on the left side of the velocity panel indicate the downhole location of the three VSP depths used. Panel six shows the reflection coefficient derived from the composite velocity and density data. The source signal that is convolved with the reflection coefficient to obtain the synthetic seismogram is shown in the top of the panel. Panel seven shows the depth-to-time conversion derived from the check shot–corrected velocity data. Bold black lines are check-shot conversions of depth to time. The synthetic seismogram is shown in panel eight (SYNT). Between panels eight and nine, the points from panel three have been projected from depth to time (and shifted down by 18 ms to account for the lag between the first break and the center of the first peak in the source signal) to enable direct correlation with the synthetic seismogram and the MCS data in panel nine. Seventy-five common midpoints (CMPs) (937.5 m) extending from Site 1118 (at CMP 4547) to the north are displayed. Key reflectors discussed in the text are annotated. LG = Light Green unit, DG = Dark Green unit. (**Figure shown on next page.**)

Figure F3 (continued). (Caption shown on previous page.)

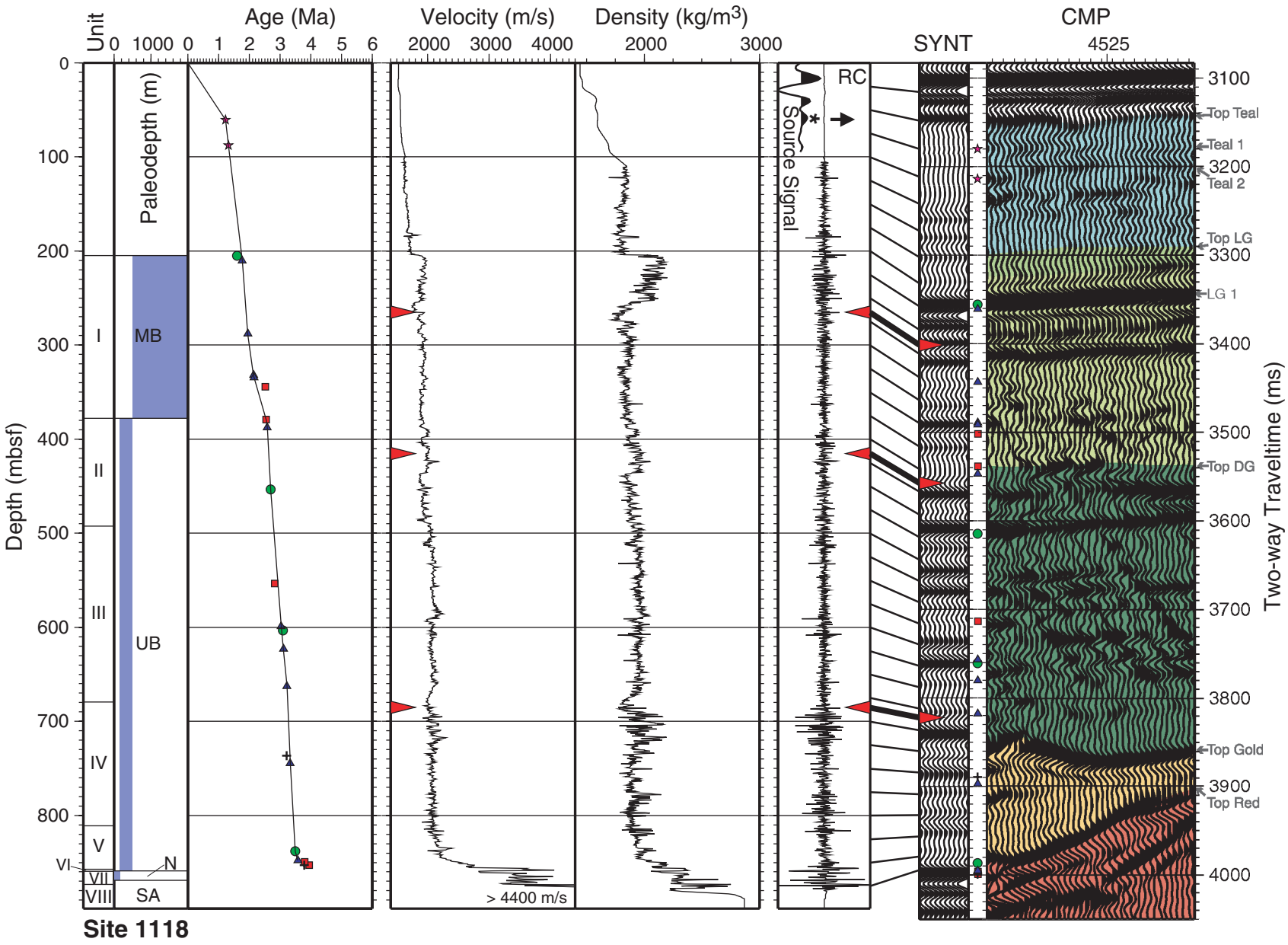

Figure F4. Logging and coring results (Shipboard Scientific Party, 1999b), check shot–corrected depth conversion, and correlation via synthetic seismogram to MCS data in the vicinity of Site 1109. Refer to the caption of Figure F3, p. 14, for a detailed explanation. In the second panel, BW = brackish water, FW = freshwater. Between panels eight and nine, the points from panel three have been projected from depth to time (and shifted down by 22 ms to account for the lag between the first break and the center of the first peak in the source signal) to enable direct correlation with the synthetic seismogram and the MCS data in panel nine. Seventy-five CMPs (937.5 m) extending from Site 1109 (at CMP 3850) to the north are displayed in panel nine. (**Figure shown on next page.**)

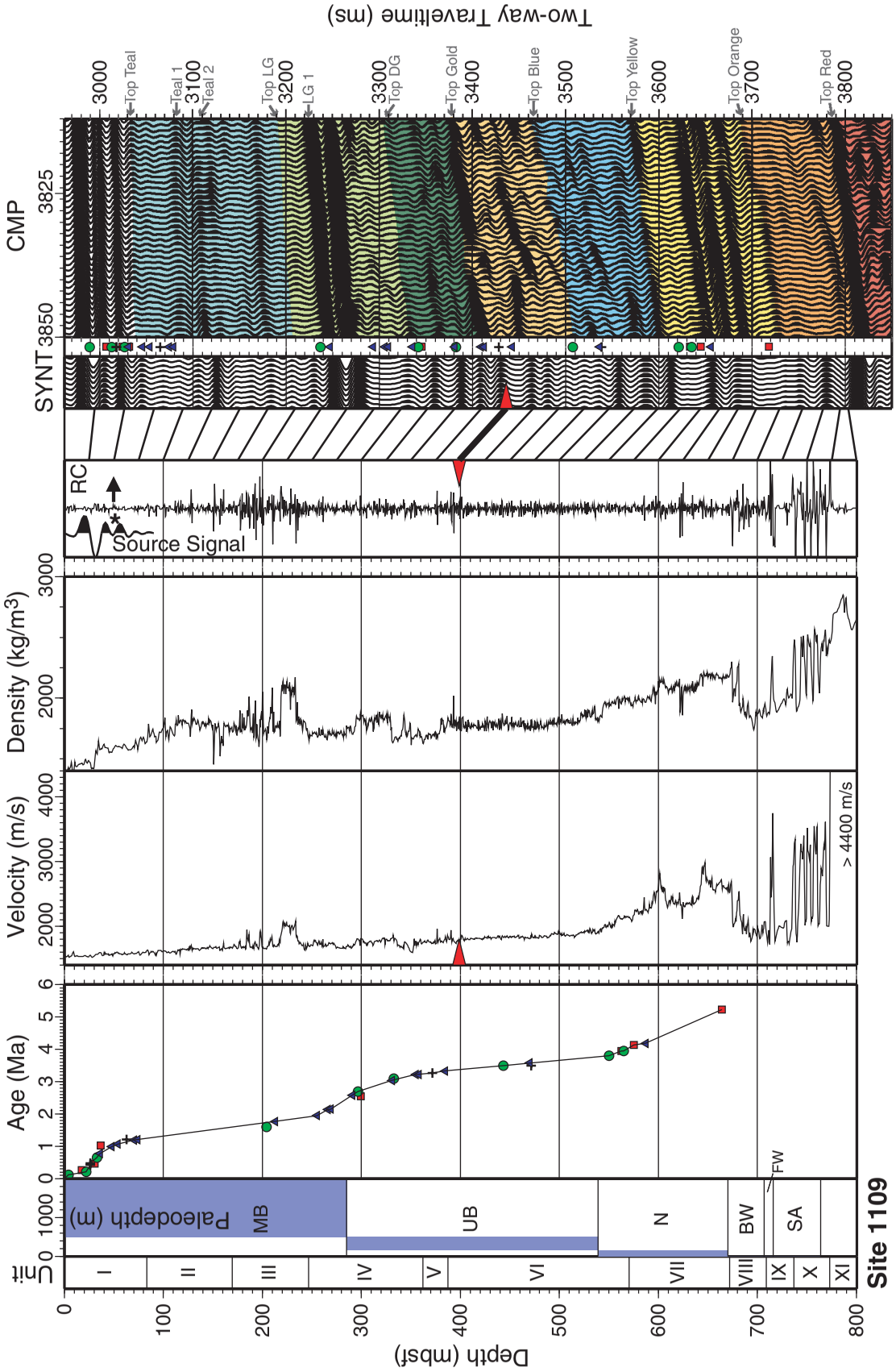

Figure F4 (continued). (Caption shown on previous page.)

Figure F5. Logging and coring results (Shipboard Scientific Party, 1999c), check shot–corrected depth conversion, and correlation via synthetic seismogram to MCS data in the vicinity of Site 1115. Refer to the caption of Figure **F3,** p. 14, for a detailed explanation. In the second panel UMB = upper middle bathyal, ON = outer neritic, IN = inner neritic, B = barren. The inset panel in the velocity panel gives age data for samples >6 Ma. Between panels eight and nine, the points from panel three have been projected from depth to time (and shifted down by 18 ms to account for the lag between the first break and the center of the first peak in the source signal) to enable direct correlation with the synthetic seismogram and the MCS data in panel nine. Seventy-five CMPs (937.5 m) extending from Site 1115 (at CMP 1050) to the north are displayed in panel nine. (**Figure shown on next page.**)

Figure F5 (continued). (Caption shown on previous page.)

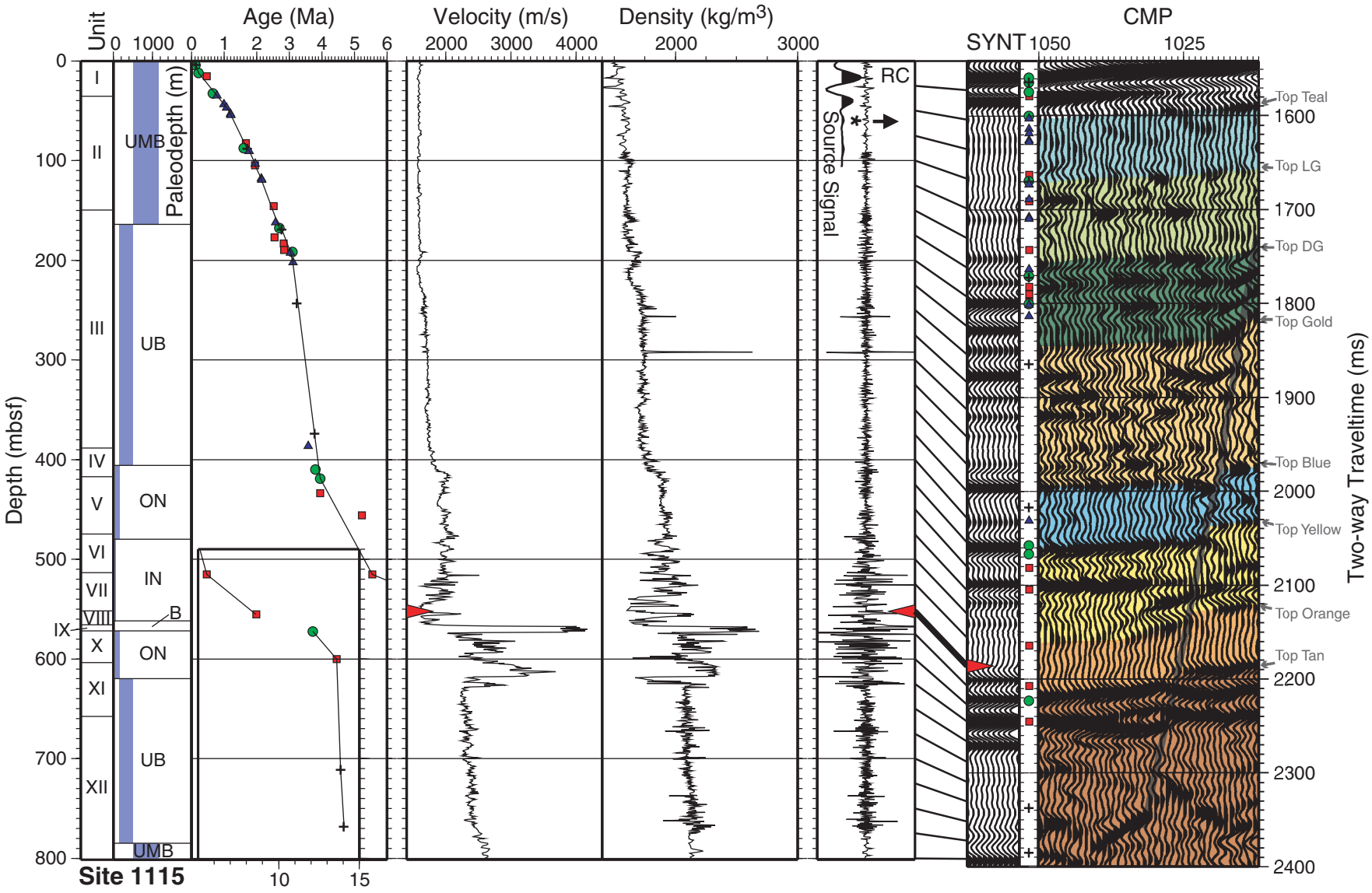

Table T1. Depth intervals over which shipboard and logging measurements of velocity were used to create composite profiles for Sites 1118, 1109, and 1115.

Site	Shipboard measurements depth (mbsf)	Logging measurements depth (mbsf)
1118	0.0–100.0*	
	874.5–899.1	100.0–874.5
1109	0.0–111.9	111.9–343.1
	343.1–385.0	385.0–768.7
	768.7–800.5	
1115	0.0–152.5	152.5–770.1
	770.1–801.5	

Note: * = Site 1109.

Table T2. Depth intervals over which shipboard and logging measurements of density were used to create composite profiles for Sites 1118, 1109, 1115.

Site	Shipboard measurements depth (mbsf)	Logging measurements depth (mbsf)
1118	0.0–110.0* 874.5–899.07	110.0–874.5
1109	0.0–111.96 81.2–800.5	111.9– 775.9
1115	0.0–92.1 774.8–801.5	92.1–774.8

Note: * = Site 1109.

Table T3. Age data, Site 1118.

Event	Depth (mbsf)	Age (Ma)	TWT (ms)
Top Teal	35.92	0.92	3148
Teal 1	60.83	1.23	3180
Teal 2	87.53	1.32	3214
Top LG	156.07	1.57	3298
LG 1	201.90	1.74	3352
3. Foraminifers	<205	1.60	<3355.5
4. Magnetic	210.42	1.77	3361.0
5. Magnetic	288.00	1.95	3443.4
6. Magnetic	332.00	2.14	3489.0
7. Magnetic	334.50	2.15	3491.5
8. Nannofossil	339.87–348.87	2.52	3497.0–3506.4
9. Nannofossil	374.47–384.20	2.55	3533.4–3543.6
Top DG	385.53	2.58	3545
10. Magnetic	387.50	2.581	3547.1
11. Foraminifers	449.93–456.85	2.70	3610.8–3617.9
12. Nannofossil	549.75–556.95	2.83	3709.9–3716.7
13. Magnetic	599.00	3.04	3756.8
14. Foraminifers	597.72–608.20	3.09	3755.6–3765.6
15. Magnetic	623.00	3.11	3780.0
16. Magnetic	662.50	3.22	3817.9
Top Gold	701.33	3.28	3856
17. $^{40}Ar/^{39}Ar$	734.90–737.70	3.21 ± 0.8	3887.9–3890.6
18. Magnetic	744.50	3.33	3897.1
19. Foraminifers	835.32–840.54	3.50	3984.0–3988.8
20. Magnetic	846.00–849.50	3.58	3993.7–3996.7
21. Nannofossil	>853.15	3.94	>3999.5
22. Foraminifers	>849.30	3.80	>3999.5
23. $^{40}Ar/^{39}Ar$	850.70–855.00	3.79 ± 0.01	3997.6–4000.8

Notes: Event numbers correspond to those presented in **Takahashi et al.,** this volume. Two-way traveltimes (TWT) of non-MCS events have had 18 ms added to move the event to the location corresponding to the point at which the first positive peak of a corresponding reflector would appear. The TWT for each event has been added, in addition to the depth, age, and TWT of key reflectors in the MCS data. Data are adapted from **Takahashi et al.,** this volume. LG = Light Green unit, DG = Dark Green unit.

Table T4. Age data, Site 1109.

Event	Depth (mbsf)	Age (Ma)	TWT (ms)
1. Foraminifers	2.43–5.39	0.12	2987.2–2991.0
2. Foraminifers	17.29–26.74	0.22	3006.4–3018.7
3. Nannofossil	17.29–17.85	0.26	3006.4–3007.2
4. $^{40}Ar/^{39}Ar$	26.26–26.28	0.43 ± 0.02	3018.1–3018.1
5. $^{40}Ar/^{39}Ar$	25.53–26.51	0.48 ± 0.04	3017.2–3018.4
6. Nannofossil	29.58–31.95	0.46	3022.44–3025.5
7. Nannofossil	32.50–32.62	0.65	3026.2–3026.4
8. Magnetic	36.00	0.78	3030.62
9. Nannofossil	36.42–36.85	1.02	3031.2–3031.7
Top Teal	41.80	0.90	3038
10. Magnetic	47.50–48.00	0.99	3045.3–3045.9
11. Magnetic	53.50–54.00	1.07	3052.9–3053.5
12. $^{40}Ar/^{39}Ar$	62.90–62.92	1.2 ± 0.16	3064.8–3064.9
13. Magnetic	70.50	1.201	3074.5
14. Magnetic	74.00	1.211	3078.9
Teal 1	79.63	1.23	3086
Teal 2	102.08	1.32	3114
Top LG	178.05	1.63	3206
15. Foraminifers	199.87–208.51	1.6	3231.4–3241.6
LG 1	210.64	1.76	3244
16. Magnetic	213.00	1.77	3246.8
17. Magnetic	255.00	1.95	3293.1
18. Magnetic	266.00	2.14	3305.9
19. Magnetic	269.00	2.15	3309.3
Top DG	289.78	2.59	3334.0
20. Nannofossil	294.81–304.36	2.55	3339.9–3350.6
21. Magnetic	291.00	2.58	3335.5
22. Foraminifers	295.75–297.23	2.7	3340.9–3342.6
23. Foraminifers	330.85–333.83	3.09	3380.5–3383.8
24. Magnetic 25	331.00	3.04	3380.7
25. Magnetic 26	355.00	3.22	3408.8
Top Gold	356.05	3.22	3410
25. Magnetic (Hole D)	358.00	3.22	3412.2
26. $^{40}Ar/^{39}Ar$	371.60–372.20	3.27 ± 0.03	3427.7–3428.4
27. Magnetic	384.50	3.33	3442.3
Top Blue	442.18	3.50	3506
28. Foraminifers	442.08–444.29	3.50	3505.9–3508.5
29. Magnetic	470.00	3.58	3536.4
30. $^{40}Ar/^{39}Ar$	471.50–471.90	3.49 ± 0.09	3538.0–3538.4
Top Yellow	529.34	3.74	3600.0
31. Foraminifers	548.80–551.00	3.8	3620.1–3622.2
32. Nannofossil	562.51–562.71	3.94	3633.3–3633.5
33. Foraminifers	562.71–566.55	3.95	3633.5–3637.1
34. Nannofossil	571.66–578.42	4.13	3641.9–3648.1
35. Magnetic	587.00	4.18	3655.8
36. Nannofossil	>664.29	5.23	>3718.2
Top Orange	676.41	>5.23	3728.0
Top Red	773.84	NA	3816.0

Notes: Event numbers correspond to those presented in **Takahashi et al.,** this volume. Two-way traveltimes (TWT) of non-MCS events have had 22 ms added to move the event to the location corresponding to the point at which the first positive peak of a corresponding reflector would appear. The TWT for each event has been added, in addition to the depth, age, and TWT of key reflectors in the MCS data. Data are adapted from **Takahashi et al.,** this volume. NA = not available. LG = Light Green unit, DG = Dark Green unit.

Table T5. Age data, Site 1115.

Event	Depth (mbsf)	Age (Ma)	TWT (ms)
1. Foraminifers	2.45–5.44	0.12	1562.2–1565.8
2. $^{40}Ar/^{39}Ar$	3.96–3.98	0.135 ± 0.008	1563.9–1564.0
3. Foraminifers	7.11–17.20	0.22	1567.8–1580.5
4. Nannofossil	14.16–17.20	0.46	1576.7–1580.5
5. Foraminifers	31.65–33.15	0.65	1598.8–1600.6
6. Magnetic	33.5–36	0.78	1601.1–1604.2
Top Teal	32.64	0.73	1604.0
7. Magnetic	43.5	0.99	1613.7–1618.1
8. Magnetic	47	1.07	1618.1
9. Magnetic	53	1.201	1625.67
10. Magnetic	54.5	1.211	1627.6
11. Foraminifers	86.65–88.35	1.6	1668.0–1670.1
12. Nannofossil	82.15–82.8	1.67	1662.3–1663.1
13. $^{40}Ar/^{39}Ar$	88.30–88.32	1.71 ± 0.06	1670.1–1670.1
14. Magnetic	90.5	1.77	1672.8
Top LG	91.42	1.79	1678
15. Magnetic	02.5–103.5	1.95	1688.0–1689.3
16. Nannofossil	103.16–106.16	1.95	1688.8–1692.7
17. Magnetic	118	2.14	1707.6
18. Magnetic	119.5	2.15	1709.5
19. Nannofossil	144.13–147.15	2.52	1740.6–1744.4
Top DG	156.38	2.54	1760
20. Magnetic	162	2.581	1763.0
21. Foraminifers	166.15–169.16	2.7	1768.3–1772.0
22. $^{40}Ar/^{39}Ar$	169.3–169.32	2.77 ± 0.04	1772.2–1772.2
23. Nannofossil	175.65–178.63	2.55	1780.2–1783.9
24. Nannofossil 25	178.63–188.15	2.83	1783.9–1795.8
25. $^{40}Ar/^{39}Ar$26	189.62–189.64	2.84 ± 0.03	1797.7–1797.7
26. Foraminifers	190.15–193.15	3.09	1798.3–1802.0
27. Magnetic	192.50	3.04	1801.2
28. Magnetic	202	3.11	1813.0
Top Gold	228.27	3.23	1850.0
29. $^{40}Ar/^{39}Ar$	243.42–243.44	3.23 ± 0.08	1864.2–1864.2
Top Blue	352.409	3.41	1996
30. $^{40}Ar/^{39}Ar$	367.9–368.6	3.78 ± 0.16	2023.4–2010.8
31. Magnetic	386.0–387.0	3.58	2030.8–2031.9
32. Foraminifers	407.31–412.07	3.8	2054.6–2059.7
Top Yellow	412.36	3.87	2064
33. Nannofossil	428.65–439.01	3.94	2076.3–2087.0
34. Foraminifers	412.07–425.81	3.95	2059.7–2073.5
35. Nannofossil	>456.04	5.23	>2104.6
Top Orange	507.32	5.39	2160
36. Nannofossil	514.29–516.37	5.54	2163.1–2165.1
37. Nannofossil	>555.29	8.6	>2207.4
38. Foraminifers	<572.27	>12.1	<2223.2
39. Nannofossil	<600.11	13.6	<2245.5
40. $^{40}Ar/^{39}Ar$	709.7–712.9	13.84 ± 0.02	2334.0–2338.7
41. $^{40}Ar/^{39}Ar$	765.4–771.8	14.04 ± 0.03	2382.6–2387.8
42. Foraminifers	<802.14	15.1	>2392.9
Top Tan	562.75	10.12	2220.0

Notes: Event numbers correspond to those presented in **Takahashi et al.,** this volume. Two-way traveltimes (TWT) of non-MCS events have had 18 ms added to move the event to the location corresponding to the point at which the first positive peak of a corresponding reflector would appear. The TWT for each event has been added, in addition to the depth, age, and TWT of key reflectors in the MCS data. Data are adapted from **Takahashi et al.,** this volume. LG = Light Green unit, DG = Dark Green unit.

CHAPTER NOTE*

N1. 19 February 2002—Lackschewitz, K., Bogaard, P.V.D., and Mertz, D.F., 2001. $^{40}Ar/^{39}Ar$ ages of fallout tephra layers and volcaniclastic deposits in the sedimentary succession of the western Woodlark Basin, Papua New Guinea: the marine record of Miocene–Pleistocene volcanism. *In* Wilson, R.C.L., Whitmarsh, R.B., Taylor, B., and Froitzheim, N. (Eds.), *Non-volcanic Rifting of Continental Margins: Evidence from Land and Sea,* Spec. Publ.—Geol. Soc. London, 187:373–388.

*Dates reflect file corrections or revisions.